A Unified Parametric Model of White Matter Fiber Tracts

University of Wisconsin, Madison
Department of Biostatistics and Medical Informatics
Technical Report 204

Moo K. Chung[1,2], Jee Eun Lee[2], Gary Park[1,2],Mariana Lazar[3], Nicholas T. Lange[5,6], Janet E. Lainhart[4], Andrew L. Alexander[2]

[1]Department of Biostatistics and Medical Informatics
[2]Waisman Laboratory for Brain Imaging and Behavior
University of Wisconsin, Madison
[3]Center for Biomedical Imaging, Department of Radiology
New York University School of Medicine, New York
[4] Department of Psychiatry
University of Utah, Salt Lake City
[5] Departments of Psychiatry and Biostatistics
Harvard University Schools of Medicine and Public Health
[6] Neurostatistics Laboratory, McLean Hospital. Boston
mkchung@wisc.edu

Abstract. We present a novel unified framework for explicitly parameterizing white fiber tracts. The coordinates of tracts are parameterized using a Fourier series expansion. For an arbitrary tract, a 19 degree cosine expansion is found to be sufficient to reconstruct the tract with an error of about 0.26 mm. By adding specific periodic constraints to open tracts, we can avoid using the sine basis. Then each tract is fully parameterized with 60 parameters, which results in a substantial data reduction. Unlike available spline models, the proposed method does not have internal knots and explicitly represents the tract as a linear combination of basis functions. This simplicity in the representation enables us to design statistical models, register tracts and segment tracts in a unified Hilbert space formulation.

1 Introduction

Diffusion tensor imaging (DTI) may be used to characterize the microstructure of biological tissues using measures of the magnitude, anisotropy and aniotropic orientation [2]. In general, it is assumed that the direction of greatest diffusivity (the major eigenvector of the diffusion tensor) is most likely aligned to the local orientation of the white matter fibers. White matter tractography offers the unique opportunity to map out, segment and characterize the trajectories

of white matter fiber bundles noninvasively in the brain. Most deterministic tractography algorithms use the local diffusion tensor orientation (primarily the major eigenvector) to estimate the local direction of propagation along the reconstructed pathway or fiber tract [3] [10] [19] [17]. Tractography has been used to visualize and map out major white matter pathways in individuals and brain atlases [7] [20] [29] [30], segment specific white matter areas for region of interest analyses [15], quantify white matter morphometry and connections [23] [27], and visualize the relationships between brain pathology (e.g., brain tumors, vascular malformations, other lesions) and white matter anatomy for clinical applications like neurosurgical planning [1] [21] [22]. However, tractography data can be challenging to interpret and quantify. Whole brain tractography studies often generate many thousand tracts and require tedious manual selection of tract groups for subsequent analyses. Recent efforts have attempted to cluster [24] and automatically segment white matter tracts [25] as well as characterize tract shape parameters [4]. Many of these techniques can be quite computationally demanding given the sizes of the data sets. Clearly efficient methods for characterizing tract shape, regional tract segmentation and clustering, tract registration, averaging and quantitation would be of tremendous value to the clinical and diffusion imaging research communities. In this study, we present a novel approach for parameterizing tract features both shape and spatial location - using Fourier descriptors.

Fourier descriptors has been previously used to classify tracts [4]. The Fourier coefficients are computed by the Fourier transform that involves the both sine and cosine series expansion. Then the sum of the squared coefficients are obtained up to degree 30 for each tract and the k-means clustering is used to classify the fibers globally. The authors conclude that a downside of using Fourier descriptors is that they are not local and it is not possible to make statement about a specific portion of the curve. Although the Fourier coefficients are global and mainly used for globally classifying shapes [28], it is still possible to obtain local shape information and make a statement about local shape characteristics [8]. In this study, we propose to use the Fourier descriptor as a parameterization for local shape representation.

3D curve matching using splines has previously been described mainly in the computer vision literature [9] [11] [16]. Unfortunately, splines are not easy to model and to manipulate explicitly as compared to Fourier descriptors due to the introduction of knots. In Clayden et al. [9], the cubic-B spline is used to parameterize the median of a set of tracts for tract dispersion modeling. Matching two splines with different numbers of knots is not computationally trivial and has been solved using a sequence of ad-hoc approaches. In Gruen et al. [11], the optimal displacement of two cubic spline curves are obtained by minimizing the sum of squared Euclidean distances. The minimization is nonlinear so an iterative updating scheme is used. On the other hand, there is no need for any numerical optimization in obtaining the displacement vectors in our method due to the very nature of the Hilbert space framework. The optimal solution is embedded in the representation itself.

Instead of using the squared distance of coordinates, others have used the curvature and torsion to find the similarity between two curves [13] [16] [18]. In [18], curvature and torsion were estimated using a finite difference scheme and the sum of the squared distance of curvature and torsion differences were minimized in an iterative fashion. Due to the space limitation, we will not consider this alternate approach.

This paper describes how to obtain local shape information employing cosine series, a special case of Fourier expansion. To our knowledge, this is the first paper that describes white fiber bundles using an *explicit* functional representation. Then using this representation, we demonstrate how to register two tracts and average multiple tracts. The ability to register tracts of varying shape and length enables us to develop a shape similarity based tract segmentation. We will further demonstrate the feasibility of this idea.

2 Methods

2.1 Image Acquisition and Processing

DTI data were acquired on a Siemens Trio 3.0 Tesla Scanner with an 8-channel, receive-only head coil. DTI was performed using a single-shot, spin-echo, EPI pulse sequence and SENSE parallel imaging (undersampling factor of 2). Diffusion-weighted images were acquired in 12 non-collinear diffusion encoding directions with diffusion weighting factor (b=0) 1000 s/mm^2 in addition to a single reference image. Data acquisition parameters included the following: contiguous (no-gap) fifty 2.5mm thick axial slices with an acquisition matrix of 128x128 over a FOV of 256mm, 4 averages, repetition time (TR) = 7000 ms, and echo time (TE) = 84 ms. Two-dimensional gradient echo images with two different echo times of 7 ms and 10 ms were obtained prior to the DTI acquisition for correcting distortions related to magnetic field inhomogenieties.

Eddy current related distortion and head motion of each data set were corrected using AIR and distortions from field inhomogeneities were corrected using custom software algorithms based on [14]. Distortion-corrected DW images were interpolated to $2 \times 2 \times 2$mm voxels and the six tensor elements were calculated using a multivariate log-linear regression method [2].

The images were isotropically resampled at 1mm^3 resolution before applying the white matter tractography algorithm. The second order Runge-Kutta streamline algorithm with tensor deflection [17] was used. The trajectories were initiated at the center of the seed voxels and were terminated if they either reached regions with the factional anisotropy (FA) value smaller then 0.15 or if the angle between two consecutive steps along the trajectory was larger than $\pi/4$. At this sampling rate, the algorithm usually produces more than 300000 tracts per brain. As an illustration, subsampled 500 tracts are shown in Figure 3. Each tract consists of 105 ± 54 control points. The distance between control points is approximately 1mm. Whole brain tracts are stored as a file of size approximately 600MB. This is a somewhat inefficient way of storing the tract

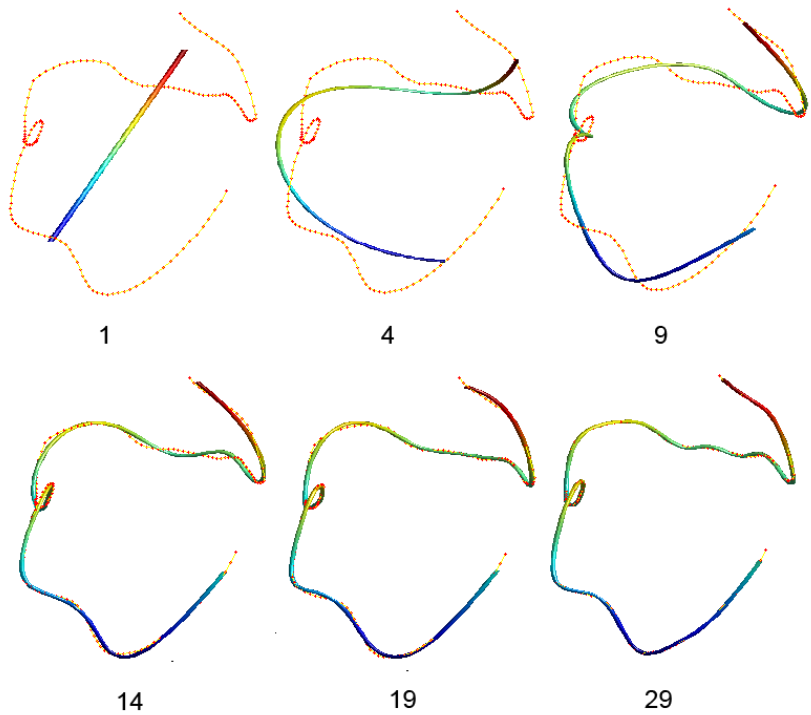

Fig. 1. Cosine series representation of a tract at various degrees. Red dots are control points. The degree 1 representation is a straight line that fits all the control points in a least squares fashion. The degree 19 representation (60 parameters) is used through out the study.

data. We present an efficient scalable data representation technique that can reduce the amount of data by a factor of 500% with a minimum loss of information. Our scalable representation can be retrieved later to give more detailed representation iteratively.

2.2 Parameterizing tracts

Consider a tract $\mathcal{M}$ consisting of n control points $p_1, \cdots, p_n$ along the tract. The second order Runge-Kutta streamline algorithm constructs tracts such that the Euclidian distance between the control points, i.e. $\|p_i - p_{i-1}\|$ is 1mm. Then we are interested in estimating a function that best represents the tract consisting of the noisy control points. This problem can be solved using piecewise continuous polynomials such as splines [26]. However, we will avoid using splines because they reintroduce control points that connect each piece of polynomials. Further, it is not straightforward to build an explicit statistical model using splines.

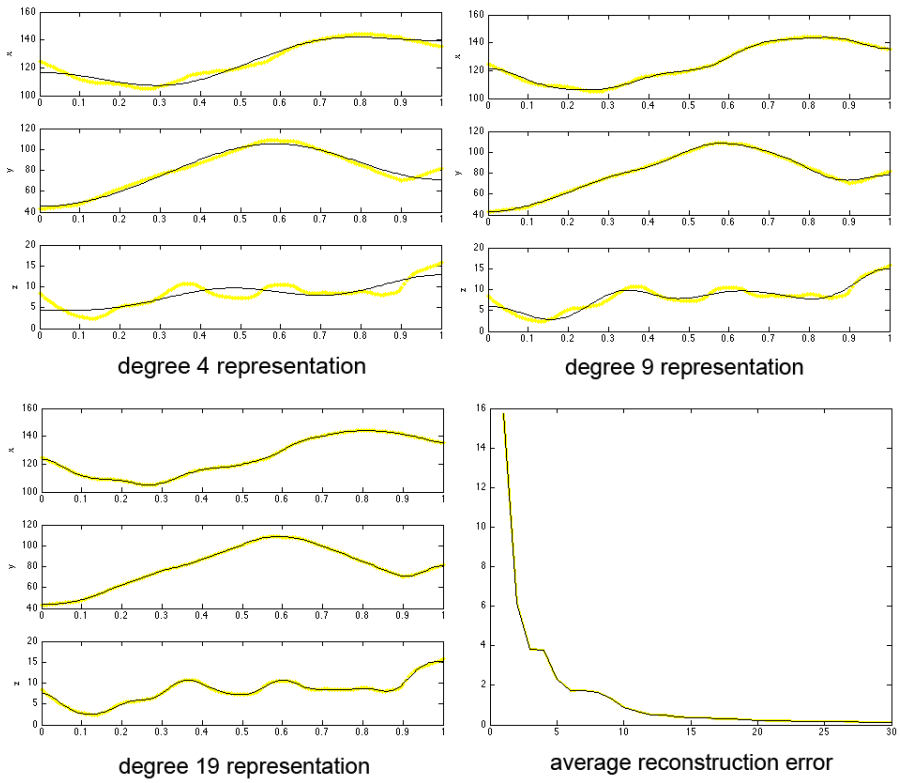

Fig. 2. The plot of x-,y- and z-coordinates over parameter space $[0, 1]$. The yellow line is the tractography result and the black line is the reconstruction at degree 9 (left) and 19 (middle). The figure in the right is the average reconstruction error over the degree of representation. The error decreases exponentially as the degree increases.

Therefore, we have developed a novel representation technique that avoids all the drawbacks of splines.

Consider a mapping ζ that maps the control point p_j onto the unit interval $[0, 1]$ as

$$\zeta : p_j \rightarrow \frac{\sum_{i=1}^{j} \|p_i - p_{i-1}\|}{\sum_{i=1}^{n} \|p_i - p_{i-1}\|} = t_j. \tag{1}$$

This is the ratio of the arc-length from the point p_1 to p_j, to p_1 to p_n. We let this ratio to be t_j. We assume $\zeta(p_1) = 0$. Then we estimate a smooth map $\zeta^{-1} : [0, 1] \rightarrow \mathcal{M}$ that passes through $\zeta^{-1}(t_j) = p_j$ in a least squares fashion.

Consider the space of square integrable functions in $[0, 1]$ denoted by $\mathcal{L}^2[0, 1]$. Let us solve the eigenequation

$$\Delta f + \lambda f = 0. \tag{2}$$

in $[0,1]$. The eigenfunctions will naturally form an orthonormal basis in $\mathcal{L}^2[0,1]$. Instead of solving (2) in the interval $[0,1]$ directly, let us solve it in $\mathbb{R}$ with the periodic constrain

$$f(t+2) = f(t).$$

Putting the periodic constrain guarantees the eigenfunctions to be the usual Fourier sine and cosine functions making numerical implementation straightforward. The reason we did not give the period 1 constraint is that it forces the function defined in $[0,1]$ to be periodic. Then from the period 2 constraint, the tract coordinates are defined only in the intervals $\cdots, [-2,-1], [0,1], [2,3] \cdots$, there is a gap in the intervals $\cdots, (-1,0), (1,2), (3,4) \cdots$. We can fill the gap by padding with zeros or some constant values but this will result in the Gibbs phenomenon (ringing artifacts) [8] at the point of discontinuity $\cdots -2, -1, 0, 1, 2, \cdots$. One way of filling the gap while making the function continuous across the whole intervals is by putting the constraint of evenness, i.e. $f(t) = f(-t)$ in the interval $[-1,0]$. The only eigenfunctions satisfying these two constraints are the cosine functions of the form

$$\psi_0(t) = 1, \psi_l(t) = \sqrt{2}\cos(l\pi t)$$

with the corresponding eigenvalues $\lambda_l = l^2\pi^2$ for integers $l > 0$. The constant $\sqrt{2}$ is introduced to make the eigenfunctions orthonormal in $[0,1]$ so that

$$\int_0^1 \psi_l(t)\psi_m(t)\, dt = \delta_{lm}. \tag{3}$$

Let $\mathcal{H}_k$ be the subspace spanned by up to the k-th degree eigenfunctions:

$$\mathcal{H}_k = \{\sum_{l=0}^{k} c_l\psi_l(t) : c_l \in \mathbb{R}\}.$$

Then we estimate a smooth function $\zeta^{-1} \in \mathcal{L}^2[0,1]$ in the subspace $\mathcal{H}_k$.

If we denote the coordinates of $\zeta^{-1}(t)$ as $(\zeta_1^{-1}, \zeta_2^{-1}, \zeta_3^{-1})$, the k-th degree *cosine series representation* of ζ^{-1} is given by

$$(\zeta_1^{-1}, \zeta_2^{-1}, \zeta_3^{-1})(t) = \sum_{l=0}^{k}(c_{l1}, c_{l2}, c_{l3})\psi_l(t). \tag{4}$$

The Fourier coefficient vectors $c_l = (c_{l1}, c_{l2}, c_{l3})$ are estimated by solving the system of equations

$$\underbrace{\begin{pmatrix} \zeta_1^{-1}(t_1) & \zeta_2^{-1}(t_1) & \zeta_3^{-1}(t_1) \\ \zeta_1^{-1}(t_2) & \zeta_2^{-1}(t_2) & \zeta_3^{-1}(t_2) \\ \vdots & \vdots & \vdots \\ \zeta_1^{-1}(t_n) & \zeta_2^{-1}(t_n) & \zeta_3^{-1}(t_n) \end{pmatrix}}_{Y} = \underbrace{\begin{pmatrix} \psi_0(t_1) & \psi_1(t_1) & \cdots & \psi_k(t_1) \\ \psi_0(t_2) & \psi_1(t_2) & \cdots & \psi_k(t_2) \\ \vdots & \vdots & \ddots & \vdots \\ \psi_0(t_n) & \psi_1(t_n) & \cdots & \psi_k(t_n) \end{pmatrix}}_{\Psi} \underbrace{\begin{pmatrix} c_{01} & c_{02} & c_{03} \\ c_{11} & c_{12} & c_{13} \\ \vdots & \vdots & \vdots \\ c_{k1} & c_{k2} & c_{k3} \end{pmatrix}}_{C}.$$

Fig. 3. Left: control points (red) obtained from the second order Runge-Kutta streamline algorithm. For visualization purpose, only 500 tracts with length larger than 50mm are shown. Yellow lines are line segments connecting consequent control points. Right: 19 degree cosine series representation of control points.

The least squares estimation is given by

$$C = (\Psi'\Psi)^{-1}\Psi' Y.$$

The proposed least squares estimation technique avoids using the Fourier transform [4] [6] [12]. The drawback of the FFT is the need for a predefined regular grid system so some sort of interpolation is needed. After various experiments, we decided to use $k = 19$ through out the paper (Figure 1). This gives the average error of 0.26mm along the tract. The plot of the average reconstruction error for other degrees is given in Figure 2 (lower right plot).

The advantage of the cosine series representation is that, instead of recording the coordinates of all control points, we only need to record $3 \cdot (k + 1)$ number of parameters for all possible tract shape. This is a substantial data reduction considering that the average number of control points is 105 (315 parameters).

2.3 Averaging White Matter Fiber Bundles

The ability to register one tract to another tract is crucial for any sort of population study, possibly via the use of the tract-based template construction. Since tracts are now represented as functions, the registration will be formulated as a minimization problem in a function space $\mathcal{H}_k$, thus avoiding numerical optimization [11] [13] [16] [18].

Suppose the Fourier representation of η^{-1} is given by

$$(\eta_1^{-1}, \eta_2^{-1}, \eta_3^{-1})(t) = \sum_{l=0}^{k} (d_{l1}, d_{l2}, d_{l3})\psi_l(t). \tag{5}$$

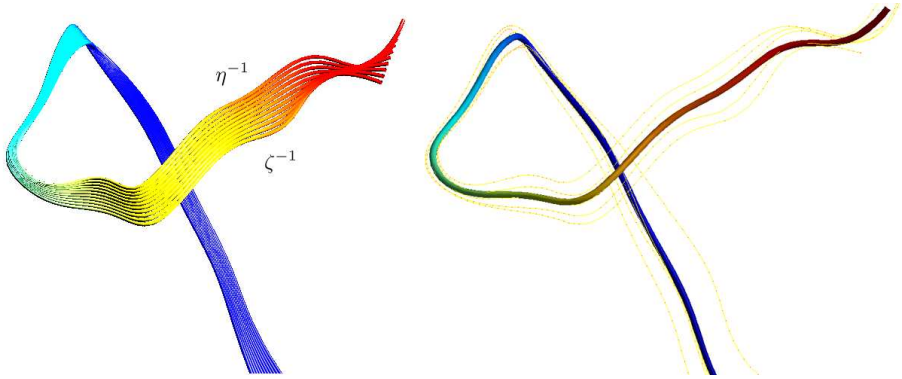

Fig. 4. Left: the trajectory of registration from ζ^{-1} to η^{-1} is represented as other intermediate tracts. The intermediate tracts are artificially generated using the optimal displacement u^*: $\zeta^{-1} + \alpha u^*$, where $\alpha \in [0, 1]$. Right: average of a bundle consisting of 5 tracts.

Let us examine how to register tract (4) to tract (5). Consider the displacement vector field $u = (u_1, u_2, u_3)$ between ζ^{-1} and η^{-1}. We will search an appropriate displacement u in the subspace $\mathcal{H}_k$ such that the discrepancy between $\zeta^{-1}(t) + u(t)$ and $\eta^{-1}(t)$ is minimized. The discrepancy ρ between two surfaces is measured as the integral of the sum of squared distance:

$$\rho(\zeta^{-1} + u, \eta^{-1}) = \int_0^1 \|\zeta^{-1}(t) + u(t) - \eta^{-1}(t)\|^2 \, dt. \tag{6}$$

Let u^* be the optimal displacement satisfying

$$u^*(t) = \arg\min_{u \in \mathcal{H}_k} \rho(\zeta^{-1} + u, \eta^{-1}).$$

Then we claim that the optimal displacement is given by

$$u^*(t) = \sum_{l=0}^{k} (d_{l1} - c_{l1}, d_{l2} - c_{l2}, d_{l3} - c_{l3}) \psi_l(t).$$

The proof requires substituting ζ^{-1} and η^{-1} with the cosine series expansion and letting

$$u(t) = \sum \sum_{l=0}^{k} (\beta_{l1}, \beta_{l2}, \beta_{l3}) \psi_l(t)$$

in the expression (6). Then the expression become the unconstrained positive definite quadratic program with respect to β_{lj}. So the global minimum always exists and obtained by differentiating with respect to β_{lj}. Note that $\rho(\zeta^{-1} + u^*, \eta^{-1}) = 0$. Figure 4 shows how the tract ζ^{-1} is registered to the other tract η^{-1}.

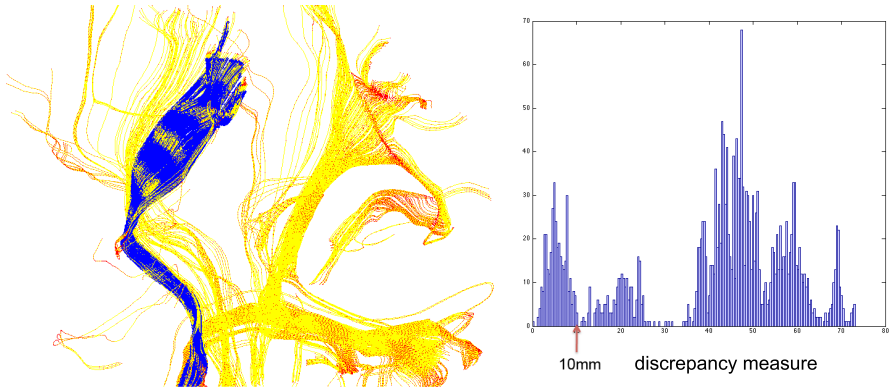

Fig. 5. Left: Right: histogram of discrepancy measure from a reference tract. Thresholding at 10mm gives the blue colored tracts.

Based on the idea of registering tracts by matching Fourier coefficients, we have constructed the average of a white fiber bundle consisting of m tracts as

$$\overline{\zeta^{-1}}(t) = \sum_{l=0}^{k} (\overline{c_{l1}}, \overline{c_{l2}}, \overline{c_{l3}}) \psi_l(t), \tag{7}$$

where $\overline{c_{li}}$ is the sample mean of the coefficients corresponding to the i-th coordinate for m tracts. As an illustration, we show how to average five tract in Figure 4.

2.4 White Matter Fiber Segmentation

Based on the discrepancy measure ρ, we have investigated the feasibility of shape-based fiber bundle segmentation. Given two cosine series representation of tracts ζ^{-1} and η^{-1}, the discrepancy measure is simplified as

$$\begin{aligned} \rho(\zeta^{-1}, \eta^{-1}) &= \int_0^1 \left\| \zeta^{-1}(t) - \eta^{-1}(t) \right\| \, dt \\ &= \int_0^1 \sum_{j=1}^{3} \left[\sum_{l=0}^{k} (c_{lj} - d_{lj}) \psi_l(t) \right]^2 \, dt \\ &= \sum_{j=1}^{3} \sum_{l=0}^{k} (c_{lj} - d_{lj})^2. \end{aligned}$$

We have used the orthonormality condition (3) in removing the integral in the expression. The advantage of our discrepancy measure is that it is automatically obtained once the cosine series representations are computed. Among 2172 tracts

visualized in Figure 5, one tract in the middle of the blue fiber bundle was selected as a reference tract ζ^{-1} then we computed the total discrepancy between the reference tract and the rest of tracts. By normalizing the discrepancy by the total arc-length of ζ^{-1}, we obtain the mean discrepancy measure along the tract. The histogram of the mean discrepancy is given in Figure 5. The histogram shows significant clustering in about 5 clusters. Since the histogram is visibly so well clustered, we did not use any automatic clustering algorithm. 357 tracts within the 10mm discrepancy error are selected and colored blue.

We have proposed a reference tract based segmentation using the discrepancy measure ρ. We can extend the proposed framework to segmenting multiple bundles. Given a collection of tracts $\zeta^{(1)}, \cdots, \zeta^{(n)}$, we measure cross discrepancy

$$\rho_{ij} = \rho(\zeta^{(i)}, \zeta^{(j)}).$$

We may need to normalize ρ_{ij} with the total arc-lengths. Then we can construct the discrepancy matrix (ρ_{ij}) and apply various classification techniques used in clustering correlation matrices [5] [31] for automatic clustering of tracts.

3 Conclusion

We have presented a unified parametric representation of white matter fiber tracts. The method explicitly models tracts using the orthonormal cosine basis. The model parameter estimation is done in the least squares fashion in a computationally efficient manner. The 19 degree representation is found to be sufficient within the 0.26mm reconstruction error. The representation will parameterize tracts of varying length and shape with 60 parameters achieving significant data reduction. The representation is used to register, average and segment tracts in a unified Hilbert space framework. Future work will attempt to use these parametric tract shape measures to perform automatic tract extraction, characterization of tract morphologic shape in different population groups, and multiple subject spatial normalization and tract segmentation.

Acknowledgement

This work was supported by NIH Mental Retardation/Developmental Disabilities Research Center (MRDDRC Waisman Center), NIMH 62015 (ALA), NIMH MH080826 (JEL) and NICHD HD35476 (University of Utah CPEA).

References

1. K. Arfanakis, M. Gui, and Lazar M. Optimization of white matter tractography for pre-surgical planning and image-guided surgery. *Oncology Report*, 15:1061–1064, 2006.
2. P.J. Basser, J. Mattiello, and D. LeBihan. MR diffusion tensor spectroscopy and imaging. *Biophys J.*, 66:259–267, 1994.

3. P.J. Basser, S. Pajevic, C. Pierpaoli, J. Duda, and A. Aldroubi. In vivo tractography using dt-mri data. *Magnetic Resonance in Medicine*, 44:625–632, 2000.
4. P.G. Batchelor, F. Calamante, J.D. Tournier, D. Atkinson, D.L. Hill, and A. Connelly. Quantification of the shape of fiber tracts. *Magnetic Resonance in Medicine*, 55:894–903, 2006.
5. P. Blinder, I. Baruchi, V. Volman, H. Levine, D. Baranes, and Jacob. E.B. Functional topology classification of biological computing networks. *Natural Computing*, 4:339–361, 2005.
6. T. Bulow. Spherical diffusion for 3d surface smoothing. *IEEE Transactions on Pattern Analysis and Machine Intelligence*, 26:1650–1654, 2004.
7. M. Catani, R.J. Howard, S. Pajevic, and D.K. Jones. Virtual in vivo interactive dissection of white matter fasciculi in the human brain. neuroimage. *NeuroImage*, 17:77–94, 2002.
8. M.K. Chung, L. Shen Dalton, K.M., A.C. Evans, and R.J. Davidson. Weighted fourier representation and its application to quantifying the amount of gray matter. *IEEE transactions on medical imaging*, 26:566–581, 2007.
9. J.D. Clayden, A.J. Storkey, and M.E. Bastin. A probabilistic model-based approach to consistent white matter tract segmentation. *IEEE Transactions on Medical Imaging*, 11:1555–1561, 2007.
10. T.E. Conturo, N.F. Lori, T.S. Cull, E. Akbudak, A.Z. Snyder, J.S. Shimony, R.C. McKinstry, H. Burton, and M.E. Raichle. Tracking neuronal fiber pathways in the living human brain. In *Natl Acad Sci USA*, volume 96, 1999.
11. A. Gruen and A. Devrim. Least squares 3d surface and curve matching. *ISPRS Journal of Photogrammetry Remote Sensing*, 59:151–174, 2005.
12. X. Gu, Y.L. Wang, T.F. Chan, T.M. Thompson, and S.T. Yau. Genus zero surface conformal mapping and its application to brain surface mapping. *IEEE Transactions on Medical Imaging*, 23:1–10, 2004.
13. A. Gueziec, X. Pennec, and N. Ayache. Medical image registration using geometeric hashing. *IEEE Computational Science and Engineering*, 4:29–41, 1997.
14. P. Jezzard and R.S. Balaban. Correction for geometric distortion in echo planar images from b0 field variations. *Magn. Reson. Med.*, 34:65–73, 2007.
15. D.K. Jones, M. Catani, C. Pierpaoli, S.J. Reeves, S.S. Shergill, M. O'Sullivan, P. Golesworthy, P. McGuire, M.A. Horsfield, A. Simmons, S.C. Williams, and R.J. Howard. Age effects on diffusion tensor magnetic resonance imaging tractography measures of frontal cortex connections in schizophrenia. *Human Brain Mapping*, 27:230–238, 2006.
16. E. Kishon, T. Hastie, and H. Wolfson. 3d curve matching using splines. In *Proceedings of the European Conference on Computer Vision*, pages 589–591, 1990.
17. M. Lazar and A.L. Alexander. Lazar, m. and weinstein, d.m. and tsuruda, j.s. and hasan, k.m. and arfanakis, k. and meyerand, m.e. and badie, b. and rowley, h. and haughton, v. and field, a. and witwer, b. and alexander, a.l. *White Matter Tractography Using Tensor Deflection*, 18:306–321, 2003.
18. A. Leemans, J. Sijbers, S. De Backer, E. Vandervliet, and P. Parizel. Multiscale white matter fiber tract coregistration: A new feature-based approach to align diffusion tensor data. *Magnetic Resonance in Medicine*, 55:1414–1423, 2006.
19. S Mori, B.J. Crain, V.P. Chacko, and P.C. van Zijl. Three-dimensional tracking of axonal projections in the brain by magnetic resonance imaging. *Annals of Neurology*, 45:256–269, 1999.
20. S. Mori, W.E. Kaufmann, C. Davatzikos, Stieljes, L. Amodei, K. Fredericksen, G.D. Pearlson, E.R. Melhem, M. Solaiyappan, G.V. Raymond, H.W. Moser, and P.C.

van Zijl. Imaging cortical association tracts in the human brain using diffusion-tensor-based axonal tracking. *Magnetic Resonance in Medicine*, 47:215–223, 2002.

21. M. Mller, J. Frandsen, G. Andersen, A. Gjedde, P. Vestergaard-Poulsen, and L. stergaard. Dynamic changes in corticospinal tracts after stroke detected by fibretracking. *Journal of Neurol. Neurosurg. Psychiatry*, 78:587–592, 2007.
22. C. Nimsky, O. Ganslandt, P. Hastreiter, R. Wang, T. Benner, A.G. Sorensen, and R. Fahlbusch. Preoperative and intraoperative diffusion tensor imaging-based fiber tracking in glioma surgery. *Neurosurgery*, 56:130–137, 2005.
23. P.G. Nucifora, R. Verma, E.R. Melhem, R.E. Gur, and R.C. Gur. Leftward asymmetry in relative fiber density of the arcuate fasciculus. *Neuroreport.*, 16:791–794, 2005.
24. L.J. O'Donnell, M. Kubicki, M.E. Shenton, M.H. Dreusicke, W.E. Grimson, and C.F. Westin. A method for clustering white matter fiber tracts. *American Journal of Neuroradiology*, 27:1032–1036, 2006.
25. L.J. O'Donnell and C.F. Westin. Automatic tractography segmentation using a high-dimensional white matter atlas. *IEEE Transactions on Medical Imaging*, 26:1562–1575, 2007.
26. S. Pajevic, A. Aldroubi, and P.J. Basser. A continuous tensor field approximation of discrete dt-mri data for extracting micro-structural and architectural features of tissues. *Journal of Magnetic Resonance*, 154:85–100, 2002.
27. T.P. Roberts, F. Liu, A. Kassner, S. Mori, and A. Guha. Fiber density index correlates with reduced fractional anisotropy in white matter of patients with glioblastoma. *American Journal of Neuroradiology*, 26:2183–2186, 2005.
28. L. Shen, J. Ford, F. Makedon, and A. Saykin. surface-based approach for classification of 3d neuroanatomical structures. *Intelligent Data Analysis*, 8:519–542, 2004.
29. P. Thottakara, M. Lazar, S.C. Johnson, and A.L. Alexander. Probabilistic connectivity and segmentation of white matter using tractography and cortical templates. *Neuroimage*, 29, 2006.
30. P.A. Yushkevich, H. Zhang, T.J. Simon, and J.C. Gee. Structure-specific statistical mapping of white matter tracts. *Neuroimage*, in press, 2008.
31. A. Zizzari, U. Sniffert, B. Michaelis, G. Gademann, and S. Swiderski. Detection of tumor in digital images of the brain. 2001.